Lattice vibrations and elastic constants of three- and two-dimensional quantal Wigner crystals near melting

1996 J. Phys.: Condens. Matter 8 8121

(http://iopscience.iop.org/0953-8984/8/43/009)

J. Phys.: Condens. Matter **8** (1996) 8121–8136. Printed in the UK

Lattice vibrations and elastic constants of three- and two-dimensional quantal Wigner crystals near melting

V Tozzini and M P Tosi

Istituto Nazionale di Fisica della Materia and Classe di Scienze, Scuola Normale Superiore, Piazza dei Cavalieri 7, I-56126 Pisa, Italy

Received 15 June 1996

Abstract. The phonon dispersion relations and the elastic constants are evaluated for Wigner electron crystals near the critical coupling strength for melting in the fully quantal regime at zero temperature. The structures considered are the body-centred and face-centred cubic lattices in dimensionality $D = 3$ and the triangular lattice in $D = 2$. The calculations are based on a density functional approach requiring as input the linear density response function of the fluid phase at freezing and the Debye–Waller factor of the crystal at melting. These are known from quantal Monte Carlo simulations both for $D = 3$ and for $D = 2$. Comparison with earlier results of harmonic calculations shows appreciable softening from anharmonicity, which is mainly associated with the exchange and correlation contributions to the effective force constants of the quantal crystal near melting. Mechanical stability of the body-centred cubic electron crystal at melting is demonstrated through a self-consistent calculation of the lattice vibrations and the mean square particle displacement entering the Debye–Waller factor, as well as by calculations of the elastic constants using the methods of long waves and of homogeneous deformations. Finally, a relationship is displayed between phonon dispersion curves in the triangular Wigner crystal near melting and plasmon excitations in the two-dimensional electron fluid near freezing.

1. Introduction

It was predicted in early work by Wigner [1, 2] that the degenerate fluid of electrons embedded in a uniform neutralizing background should crystallize at sufficiently low density in a body-centred cubic (BCC) lattice, as an extreme consequence of correlations induced in the electronic motions by their Coulomb repulsive interactions. Quantal Monte Carlo (QMC) simulations by Ceperley and Alder [3] later established that, at $r_s \approx 100$, the BCC electron crystal becomes energetically favoured relative to the spin-polarized fluid, this fluid state being lower in energy with respect to the unpolarized fluid for $r_s > 75$. As usual, r_s is a dimensionless length related to the electron density n in dimensionality $D = 3$ by $r_s a_0 = (4\pi n/3)^{-1/3}$ with a_0 the Bohr radius. QMC work has also established a similar phase behaviour for a degenerate system of electrons in $D = 2$ with e^2/r interactions, crystallizing into a triangular lattice at $r_s \approx 35$ with $r_s a_0 = (\pi n)^{-1/2}$ in this case [4, 5].

Early theoretical attempts to assess the density range of mechanical stability for ideal Wigner crystals were based on self-consistent calculations of the effects of anharmonicity on their vibrational properties, as presented for the BCC crystal by Kugler [6] and for the triangular crystal by Platzman and Fukuyama [7]. Kugler evaluated first the vibrational frequencies of the crystal in a renormalized harmonic approximation (RHA) neglecting inter-site correlations. In the RHA the mean square displacement of a particle in its vibrational

0953-8984/96/438121+16$19.50

motion around its lattice site enters the dynamical matrix and is self-consistently determined from the inverse first moment of the vibrational spectrum. Kugler found that a self-consistent solution of the RHA could be obtained down to $r_s = 21.9$, at which an instability of the BCC lattice arose, leading to a discontinuous vanishing of the crystalline order parameters in a first-order transition to a fluid phase. The RHA calculations of Platzman and Fukuyama for the triangular lattice similarly admit a self-consistent solution down to $r_s = 4.5$. Thus, in both cases the predicted stability limit of the crystal safely lies at much higher density than that for thermodynamic melting in the QMC work. However, for the BCC crystal Kugler also tried to evaluate higher order anharmonic effects, including some account of inter-site correlations. He found from these calculations that deviations from harmonicity could set in at much larger values of r_s, leading to instability of the BCC lattice for $r_s < 700$.

Recent developments in density functional theory (DFT) offer the possibility of evaluating the anharmonic vibrational frequencies in the crystal near melting directly from properties of the fluid phase near freezing, rather than from an interatomic potential energy function treated by an anharmonic expansion (see Tosi and Tozzini [8] and references given therein). This approach assumes that the bonding character is not changed across melting and that the effective force constants in the crystal near melting are described by a Fourier-transformable central field, with Fourier transform $F(k)$ say. The simplest DFT calculation of $F(k)$ expresses it through the density reponse function of the fluid phase and the Debye–Waller factor of the crystalline phase. For a quantal Wigner crystal [9] the structure of the renormalized phonon dispersion curves is thus similar to that obtained in the self-consistent phonon theories, with exchange and correlation being included through recourse to the density response function of the fluid. Correlations are crucially important at large r_s, at which they drive Wigner crystallization.

We present in this work DFT calculations of the renormalized phonon dispersion curves and the elastic constants for the BCC and the face-centred cubic (FCC) Wigner crystals in $D = 3$ and for the triangular Wigner lattice in $D = 2$. The essential input is taken from QMC work on the density response function of the electron fluid in $D = 2$ [10] and $D = 3$ [11] and on the mean square displacements in Wigner crystals [4, 12]. Exchange and correlation enter the theory primarily through the so-called local field factor $G(k)$ from the dielectric screening theory of the electron gas [13]. Thus, the present work also tests and refines our earlier results for the BCC crystal [9], for which QMC values of $G(k)$ were not yet available so that only an estimate of this function could be constructed from its known asymptotic behaviours.

The consequence of exchange and correlation is to induce an effective attraction between the electrons and hence an anharmonic softening of the vibrational frequencies, as already suggested by the aforementioned work of Kugler. We examine with particular care below the question of the mechanical stability of Wigner crystals, in terms of two main aspects: (i) consistency between the renormalized vibrational spectrum and the mean square displacement and (ii) stability under elastic deformations. In the latter respect we evaluate the elastic constants by two alternative methods, from the long-wavelength limit of the vibrational dispersion curves (the method of long waves, or LW) and from a calculation of the energy change accompanying static homogeneous deformations (the HD method). Consistency between the results obtained by these two methods is a primary issue in the microscopic theory of the elasticity of crystals [14].

The lay-out of the paper is briefly as follows. The theory behind the calculations of vibrational frequencies and elastic constants of a quantal crystal near melting is presented in section 2 and in two appendices. Sections 3 and 4 report our results for 3D and 2D Wigner crystals, respectively. Section 5 offers a summary of our results and our main conclusions.

2. The DFT approach to vibrational frequencies and elastic constants of quantal crystals at melting

The Hohenberg–Kohn theorem for a many-body system at zero temperature in an external potential $v(\boldsymbol{r})$ allows one to define uniquely a functional $E[n(\boldsymbol{r})]$ of the one-body density $n(\boldsymbol{r})$, which is minimized by the ground-state density and takes at that density the value of the ground-state energy. We write

$$E[n(\boldsymbol{r})] = T_0[n(\boldsymbol{r})] + \int \mathrm{d}\boldsymbol{r} n(\boldsymbol{r}) v(\boldsymbol{r}) + E_{ex}[n(\boldsymbol{r})] \tag{1}$$

where $T_0[n(\boldsymbol{r})]$ is the ideal-gas kinetic energy functional and $E_{ex}[n(\boldsymbol{r})]$ is the excess (Hartree plus exchange and correlation) energy functional. The equilibrium condition can be written as

$$\begin{aligned} \frac{\delta T_0[n(\boldsymbol{r})]}{\delta n(\boldsymbol{r})} &= \mu - v(\boldsymbol{r}) - \frac{\delta E_{ex}[n(\boldsymbol{r})]}{\delta n(\boldsymbol{r})} \\ &\equiv \mu - v_{KS}(\boldsymbol{r}) \end{aligned} \tag{2}$$

where μ is the chemical potential and $v_{KS}(\boldsymbol{r})$ is the Kohn–Sham effective one-body potential.

In the present case $v(\boldsymbol{r})$ is a potential which acts on a crystal to deform it by generating a wave of lattice site displacements of arbitrarily small amplitude. This potential does not need to be specified in evaluating the corresponding change $\Delta\Omega$ in the grand thermodynamic potential $\Omega = E - \mu N$, to quadratic terms in the displacement amplitude [15]. From equations (1) and (2) we can write

$$\Omega = \Omega_0 + \Omega_{ex} \tag{3}$$

where

$$\Omega_0 = T_0[n(\boldsymbol{r})] - \int \mathrm{d}\boldsymbol{r}\, n(\boldsymbol{r}) \frac{\delta T_0[n(\boldsymbol{r})]}{\delta n(\boldsymbol{r})} \tag{4}$$

$$\Omega_{ex} = E_{ex}[n(\boldsymbol{r})] - \int \mathrm{d}\boldsymbol{r}\, n(\boldsymbol{r}) \frac{\delta E_{ex}[n(\boldsymbol{r})]}{\delta n(\boldsymbol{r})}. \tag{5}$$

The work associated with the deformation is then obtained as

$$\Delta\Omega = \Delta\Omega_0 + \Delta\Omega_{ex} \tag{6}$$

the differences being taken between the deformed and undeformed crystal with equilibrium density profiles $n_d(\boldsymbol{r})$ and $n_0(\boldsymbol{r})$, respectively.

In the case of a Wigner crystal the ideal term $\Delta\Omega_0$ in equation (6) is estimated by two alternative approximations in appendix 1 and shown to be essentially negligible in the present context. On the other hand, we treat the excess energy functional by a quadratic functional expansion both of the deformed and of the undeformed crystal around the homogeneous fluid phase, with the result

$$\Delta\Omega_{ex} = -\frac{1}{2} \iint \mathrm{d}\boldsymbol{r}_1\, \mathrm{d}\boldsymbol{r}_2 \left. \frac{\delta^2 E_{ex}[n(\boldsymbol{r})]}{\delta n(\boldsymbol{r}_1)\delta n(\boldsymbol{r}_2)} \right|_{n(\boldsymbol{r})=n} [n_d(\boldsymbol{r}_1) n_d(\boldsymbol{r}_2) - n_0(\boldsymbol{r}_1) n_0(\boldsymbol{r}_2)]. \tag{7}$$

The functional derivative in equation (7) is taken on the homogeneous fluid phase near crystallization. It is immediately related in Fourier transform to the static density response

function $\chi(k)$ of the fluid phase and to the static Lindhard susceptibility $\chi_0(k)$, and hence to the static local field factor $G(k)$ for exchange and correlation:

$$FT\left(\frac{\delta^2 E_{ex}[n(\boldsymbol{r})]}{\delta n(\boldsymbol{r}_1)\delta n(\boldsymbol{r}_2)}\bigg|_{n(\boldsymbol{r})=n}\right) = n\left(\frac{1}{\chi_0(k)} - \frac{1}{\chi(k)}\right) = \phi(k)[1 - G(k)]. \tag{8}$$

Here, $\phi(k)$ is the Fourier transform of the Coulomb potential, given by $\phi(k) = 4\pi ne^2/k^2$ in $D = 3$ and by $\phi(k) = 2\pi ne^2/k$ in $D = 2$.

2.1. Vibrational frequencies

The set of lattice site displacements $\boldsymbol{d}_R$ in the deformed crystal is taken as a static wave corresponding to a phonon of wavevector $\boldsymbol{q}$ and branch index s, with eigenvector $\hat{\varepsilon}_{qs}$ and eigenfrequency ω_{qs}. The work associated with the deformation is $\Delta\Omega = -m\omega_{qs}^2\alpha^2/4$, where m is the electron mass and α is the amplitude of the displacement wave. Comparing this with the result in equations (6)–(8) and using a Gaussian approximation for the fluctuations of the electron density around each lattice site, one obtains the dispersion relation [9]

$$\omega_{qs}^2 = F(q)(\boldsymbol{q}\cdot\hat{\varepsilon}_{qs})^2 + \sum_{\boldsymbol{K}\neq 0}\{F(|\boldsymbol{q}+\boldsymbol{K}|)[(\boldsymbol{q}+\boldsymbol{K})\cdot\hat{\varepsilon}_{qs}]^2 - F(K)(\boldsymbol{K}\cdot\hat{\varepsilon}_{qs})^2\}. \tag{9}$$

In equation (9) $\boldsymbol{K}$ denotes the reciprocal vectors of the lattice and $F(k)$ is given by

$$F(k) = \frac{1}{m}\phi(k)f^2(k)[1 - G(k)]. \tag{10}$$

Here $f(k)$ is the Debye–Waller factor of the crystal at melting, which is given by

$$f(k) = \exp\left(-\frac{1}{2D}k^2L^2d^2\right) \tag{11}$$

in terms of the Lindemann parameter $L = \langle u^2\rangle^{1/2}/d$, with $\langle u^2\rangle$ the mean square displacement at melting and d the first-neighbour distance. The factor $f^2(k)$ ensures rapid convergence of the sum in equation (9).

In summary, while the structure of the dispersion relation in equation (9) is determined by the crystalline translational symmetry, the DFT calculation leads to the approximate expression in equation (10) for the effective force constants of the crystal near melting. The essential input is provided by the static local field factor $G(k)$ for exchange and correlation and by the Lindemann parameter L. It is shown in appendix 2 that the RHA results of Kugler [6] are recovered by setting $G(k) = 0$ in equation (10). The possibility of a self-consistent evaluation arises from the fact that the Lindemann parameter is related to the inverse first moment of the vibrational spectrum by

$$L^2 = \frac{\hbar}{2Nmd^2}\sum_{qs}\frac{1}{\omega_{qs}} \tag{12}$$

N being the number of vibrational modes contained in the first Brillouin zone. Equation (12) applies in the extreme quantal limit of present interest and is free from long-wavelength divergence in $D = 2$.

As a last remark, by summing equation (9) over the three phonon branches in $D = 3$ we find

$$\sum_s \omega_{qs}^2 = \omega_p^2 + \sum_{\boldsymbol{K}}[(\boldsymbol{q}+\boldsymbol{K})^2F(|\boldsymbol{q}+\boldsymbol{K}|) - K^2F(K)] \tag{13}$$

with $\omega_p = (4\pi ne^2/m)^{1/2}$. The sum on the right-hand side of equation (13) represents a deviation from the Kohn sum rule, which is due to anharmonicity. Indeed, in the harmonic limit equation (9) holds with $F(k) \to \phi(k)/m$ and hence

$$\sum_s \omega_{qs}^2 \to \omega_p^2.$$

2.2. Elastic constants by the LW method

The shear elastic constants are obtained from equation (9) by taking the long-wavelength limit on transverse modes propagating along suitable symmetry directions. We define

$$D(k) = \frac{1}{2}k\frac{\mathrm{d}F(k)}{\mathrm{d}k}$$
$$E(k) = \frac{1}{2}k^2\frac{\mathrm{d}^2F(k)}{\mathrm{d}k^2}.$$

For a cubic crystal we find

$$\frac{c_{44}}{nm} = \sum_{\boldsymbol{K}\neq 0}\left(\frac{1}{3}D(K) + \frac{K_x^2K_y^2}{K^4}[E(K) - D(K)]\right) \tag{14}$$

from the case $\hat{\boldsymbol{q}} = [100]$ and $\hat{\varepsilon}_{qs} = [001]$, and

$$\frac{c_{11} - c_{12}}{2nm} = \sum_{\boldsymbol{K}\neq 0}\left(\frac{1}{3}D(K) + \frac{1}{2}\frac{K_x^4 - K_x^2K_y^2}{K^4}[E(K) - D(K)]\right) \tag{15}$$

from the case $\hat{\boldsymbol{q}} = [110]$ and $\hat{\varepsilon}_{qs} = [1\bar{1}0]$. Similarly, the shear modulus of the triangular lattice is given by

$$\frac{c_{33}}{nm} = \sum_{\boldsymbol{K}\neq 0}\left(\frac{1}{2}D(K) + \frac{K_x^2K_y^2}{K^4}[E(K) - D(K)]\right). \tag{16}$$

On the other hand, the longitudinal modes of a Wigner crystal have optical character and the long-wavelength limit, taken along a symmetry direction $\hat{\boldsymbol{q}}$ yields

$$\omega_{qL}^2 \to \omega_p^2 + A_{\hat{q}}q^2. \tag{17}$$

Here, ω_p is the plasma frequency in the limit $q \to 0$, which is given by $\omega_p = (4\pi ne^2/m)^{1/2}$ in $D = 3$ and $\omega_p = (2\pi ne^2q/m)^{1/2}$ in $D = 2$. For the leading dispersion coefficient $A_{\hat{q}}$ we find

$$A_{[100]} = \frac{1}{2}\frac{\mathrm{d}^2[k^2F(k)]}{\mathrm{d}k^2}\bigg|_{k=0} + \sum_{\boldsymbol{K}\neq 0}\left(F(K) + \frac{5}{3}D(K) + \frac{K_x^4}{K^4}[E(K) - D(K)]\right) \tag{18}$$

along the [100] direction in a cubic lattice and

$$A_{[10]} = \frac{1}{2}\frac{\mathrm{d}^2[k^2F(k)]}{\mathrm{d}k^2}\bigg|_{k=0} + \sum_{\boldsymbol{K}\neq 0}\left(F(K) + \frac{5}{2}D(K) + \frac{K_x^4}{K^4}[E(K) - D(K)]\right) \tag{19}$$

along the [10] direction in the triangular lattice.

2.3. Elastic constants by the HD method

No charge separation accompanies a static homogeneous deformation of a Wigner crystal, so that the HD method can be used to obtain an expression for the longitudinal elastic constant c_{11} in addition to expressions for the shear elastic constants. Following the treatment summarized by Ramakrishnan [16], the results are

$$\frac{c_{11}}{nm} = \sum_{\boldsymbol{K}\neq 0}\left(D(K) + \frac{K_x^4}{K^4}[E(K) - D(K)]\right) \tag{20}$$

$$\frac{c_{44}}{nm} = \sum_{\boldsymbol{K}\neq 0}\left(D(K) + \frac{K_x^2 K_y^2}{K^4}[E(K) - D(K)]\right) \tag{21}$$

$$\frac{c_{12}}{nm} = \sum_{\boldsymbol{K}\neq 0}\frac{K_x^2 K_y^2}{K^4}[E(K) - D(K)] \tag{22}$$

for a cubic crystal, whereas for the triangular lattice we find

$$\frac{c_{11}}{nm} = \sum_{\boldsymbol{K}\neq 0}\left(\frac{3}{2}D(K) + \frac{K_x^4}{K^4}[E(K) - D(K)]\right) \tag{23}$$

$$\frac{c_{33}}{nm} = \sum_{\boldsymbol{K}\neq 0}\left(\frac{3}{2}D(K) + \frac{K_x^2 K_y^2}{K^4}[E(K) - D(K)]\right). \tag{24}$$

We notice that there are differences between these results and those given in equations (14)–(16) above. These differences are determined by the values of $D(K)$ and will therefore be small if the reciprocal-lattice vectors lie in approximate correspondence with the extrema of the function $F(k)$. This is the case for the BCC Wigner crystal.

3. Results for cubic electron crystals

We report in this section our results for the electron crystal at $r_s = 100$ both for the BCC and for the FCC structure. Our starting value for the Lindemann parameter is $L = 0.30$, as obtained from QMC work on the BCC structure [12, 3]. DFT calculations of the freezing transition by Senatore and Pastore [17] have shown that the equilibrium density profile of the crystal near melting is well represented by a superposition of Gaussian clouds centred on the lattice sites, with $L = 0.34$ for the BCC structure and $L = 0.39$ for the FCC structure.

With regard to the local field factor $G(k)$, we have already emphasized in our earlier work [9] the sensitivity of the calculated phonon dispersion curves and elastic constants to the incorporation of the known asymptotic behaviours of this function both at low k and large k. These behaviours are reported in appendix 3 and are shown by the two dotted curves in figure 1. The broken curve in figure 1 shows our earlier attempt to interpolate between the two asymptotic behaviours, in comparison with QMC data for the spin-polarized electron fluid at $r_s = 100$ which have kindly been made available to us by Dr S Moroni (see also [11]). The full curve in figure 1 shows the interpolation of the QMC data that we have adopted for the purposes of the present calculations. However, we shall also use our earlier estimate (indicated in the following by $G_{est}(k)$) in order to illustrate the sensitivity of the results to the details of the local field factor.

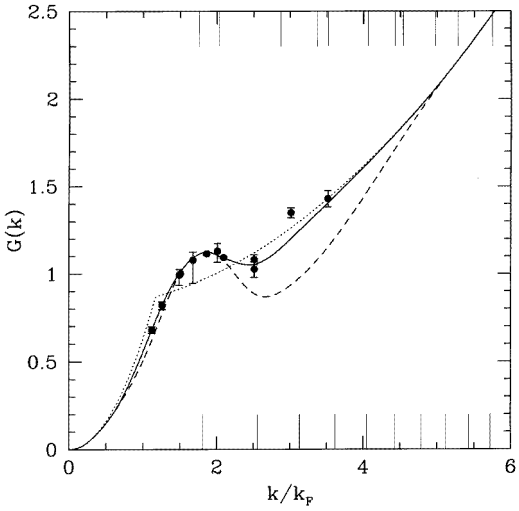

Figure 1. The local field factor $G(k)$ versus k/k_F for the spin-polarized electron fluid in $D = 3$ at $r_s = 100$. Dots with error bars are from QMC work of S Moroni (to be published) and the full curve is an interpolation fit accounting for the asymptotic behaviours shown by the dotted curves. The broken curve shows an earlier estimate of $G(k)$ for phonon calculations [9]. The vertical bars show the locations of the stars of reciprocal-lattice vectors for the BCC lattice (bottom) and for the FCC lattice (top).

3.1. The BCC crystal

Figure 2 reports the calculated phonon dispersion curves along the main symmetry directions in the BCC crystal at $r_s = 100$. The differences between the two forms of $G(k)$ given in figure 1 mainly affect the phonon frequencies near the boundaries of the Brillouin zone by amounts of at most 10%. The results are quite sensitive to the details of the force constants in the region $k \approx k_F$.

Figure 2 also compares our results with the phonon dispersion curves evaluated by earlier authors [18–20] in the harmonic approximation. This is recovered by taking $L = 0$ and $G(k) = 0$ in equations (9) and (10). It is evident that there is quite an appreciable softening from anharmonicity in most of the phonon branches and especially in the transverse ones.

From the phonon frequencies shown in figure 2 we re-evaluated the Lindemann parameter L by means of equation (12), using the Houston method [21, 22] to perform the spectral sum from knowledge of the dispersion curves along the main symmetry directions. The calculation was then continued up to self-consistency between the input value of L and that obtained from the phonon frequencies. The value of the Lindemann parameter at convergence is $L = 0.34$ for both choices of the local field factor shown in figure 1. Such a small shift from the initial input value taken from the QMC data implies only minor shifts of the phonon dispersion curves relative to those shown in figure 2. An increase in the value of L generally tends to enhance the anharmonic softening of the vibrational modes, but an instability of the BCC lattice would ensue only at much larger values of this parameter.

Table 1 reports the calculated elastic constants and plasmon dispersion coefficient for the BCC Wigner crystal at $r_s = 100$. The results show little sensitivity to the details of the local field factor and there is excellent agreement between the outputs of the LW and the HD method. As already remarked in section 2 the consistency between the two methods

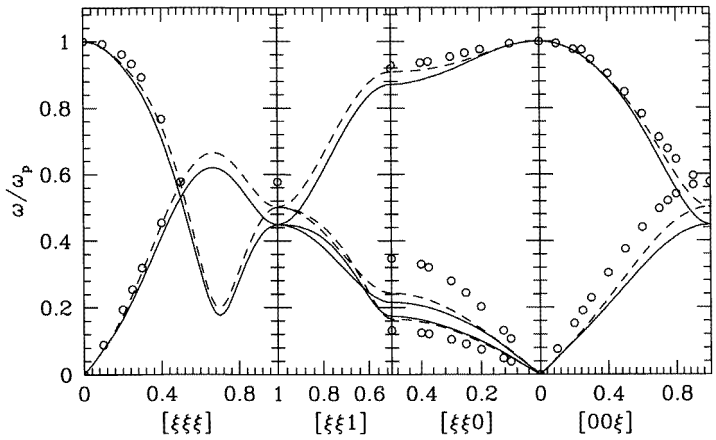

Figure 2. Phonon dispersion relations of the BCC electron lattice at $r_s = 100$ from $G_{QMC}(k)$ (full curves) and from $G_{est}(k)$ (broken curves), compared with the results of harmonic calculations (circles). The direction of the wavevector $\boldsymbol{q}$, with components in units of $\pi\sqrt{3}/d$, is shown below the graph. The frequencies are plotted as functions of ξ and are in units of the plasma frequency.

Table 1. Elastic constants c_{ij} (in units of $nm\omega_p^2/k_F^2$) and the plasmon dispersion coefficient $A_{[100]}$ (in units of ω_p^2/k_F^2) for the BCC Wigner electron lattice at $r_s = 100$.

		c_{11}	c_{44}	c_{12}	$c_{11}-c_{12}$	$A_{[100]}$
$G_{QMC}(k)$	LW		0.141		0.160	−1.70
	HD	0.300	0.152	0.078	0.222	
G_{est}(k)	LW		0.158		0.159	−1.68
	HD	0.318	0.159	0.156	0.162	

hinges on the fact that the extrema in the field of force constants $F(k)$ are in good register with the reciprocal-lattice vectors of the BCC lattice, so that the magnitude of the quantities $D(K)$ is effectively negligible in this case.

3.2. The FCC crystal

Figure 3 reports the phonon dispersion curves for an electron crystal in the FCC structure, calculated at $r_s = 100$ with $L = 0.30$. The softening of the phonon branches from anharmonicity and their sensitivity to the details of the local field factor are illustrated as in figure 2. It is seen from figure 3 that the instability of a transverse phonon branch near the zone centre in the [110] direction that we reported in our earlier work [9] is confirmed by the present calculations. As recalled at the beginning of this section, the DFT calculations of Senatore and Pastore [17] yield $L = 0.39$ in this case and thus do not support the appreciable lowering of the Lindemann parameter that would be necessary to stabilize this structure.

The corresponding results for the mechanical and long-wavelength properties of the FCC lattice are shown in table 2. The lattice is unstable against a $(c_{11} - c_{12})$ shear both in the LW and in the HD calculation. The two methods yield substantially consistent results when the local field factor $G(k)$ is taken from the QMC data. In this case the HD calculation

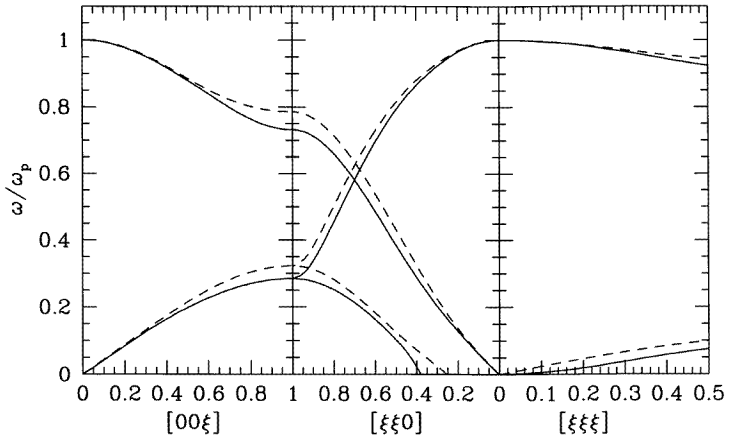

Figure 3. Phonon dispersion relations of the FCC electron lattice at $r_s = 100$ from $G_{QMC}(k)$ (full curves) and from $G_{est}(k)$ (broken curves). The direction of the wavevector $\boldsymbol{q}$, with components in units of $\pi\sqrt{2}/d$, is shown below the graph. The frequencies are plotted as functions of ξ and are in units of the plasma frequency.

Table 2. Elastic constants c_{ij} (in units of $nm\omega_p^2/k_F^2$) and the plasmon dispersion coefficient $A_{[100]}$ (in units of ω_p^2/k_F^2) for the FCC Wigner electron lattice at $r_s = 100$.

		c_{11}	c_{44}	c_{12}	$c_{11} - c_{12}$	$A_{[100]}$
$G_{QMC}(k)$	LW		0.171		−0.158	−2.32
	HD	0.012	0.176	0.159	−0.147	
$G_{est}(k)$	LW		0.184		−0.245	−1.98
	HD	0.169	0.198	0.184	−0.016	

shows that the mechanical instability of the FCC lattice arises from a very low value of the elastic constant c_{11}. Table 2 also shows that the value of this elastic constant is very sensitive to the choice of the local field factor. This sensitivity is associated with the (200) star of reciprocal-lattice vectors of the FCC structure, giving from the geometrical factors in equations (20)–(22) a large contribution to c_{11} but no contribution to the shear elastic constants.

4. Results for the triangular electron crystal

The QMC work on the triangular Wigner lattice [4, 5] indicates that the value $L \approx 0.3$ is again appropriate near melting in the fully quantal regime. Figure 4 reports the basic input concerning the local field factor $G(k)$ for the electron fluid in $D = 2$ with e^2/r interactions. Circles and triangles are from QMC work on the spin-polarized and unpolarized fluid at $r_s = 40$, respectively, as kindly made available to us by Dr S Moroni (see also [10]). Figure 4 also shows the asymptotic behaviours of $G(k)$ from the expressions reported in appendix 3 and the interpolation fits that we have adopted in the calculations reported below.

Figure 5 shows our results for the phonon dispersion curves in the triangular lattice at $r_s = 40$ as calculated from the two forms of $G(k)$ reported in figure 4. They are compared with the results of calculations by Bonsall and Maradudin [23] in the harmonic

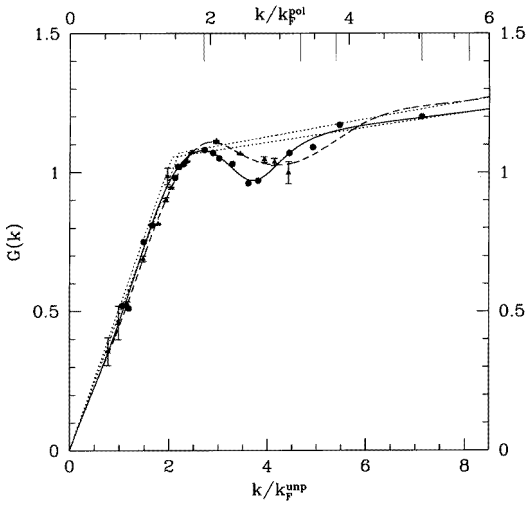

Figure 4. The local field factor $G(k)$ versus k/k_F for the electron fluid in $D = 2$ at $r_s = 40$. Dots are from QMC work of S Moroni (to be published) for the spin-polarized fluid and the full curve is an interpolation fit accounting for the asymptotic behaviours shown by the dotted curves. The triangles with error bars and the broken curve give the corresponding data for the unpolarized fluid, with the appropriate asymptotic behaviours. The vertical bars at the top show the locations of the stars of reciprocal-lattice vectors for the triangular lattice.

approximation. The longitudinal branches start at the zone centre with the characteristic 2D behaviour $\omega(q \to 0) = (2\pi ne^2 q/m)^{1/2}$ and show only small shifts from anharmonicity at finite wavenumber. There is instead an appreciable anharmonic softening in the transverse branches. In recent calculations by Esfarjani and Chui [24] it was found that both longitudinal and transverse branches are softened by anharmonicity when cubic corrections are perturbatively added onto an RHA calculation, the effects on the transverse branches being quantitatively similar to those shown in figure 5 from the spin-polarized fluid data.

For the triangular lattice we have not succeeded in bringing to convergence a self-consistent calculation of the phonon frequencies and the Lindemann parameter. A somewhat lower initial value of L would in this respect be more appropriate than the value $L = 0.30$ within the present theoretical approach, but still does not allow convergence to be reached at $r_s = 40$. At such values of L the triangular lattice is nevertheless stable against elastic deformations, as can be seen from the results on the elastic constants in table 3. At the quantitative level the calculated elastic constants are seen from table 3 to be very sensitive to the input data on the local field factor (spin-polarized versus unpolarized fluid) and to the method used in their evaluation (LW versus HD). All these results can be explained *a posteriori* from the relative locations of the extrema in $F(k)$ and the reciprocal vectors of the triangular lattice.

4.1. The relation to plasmon excitation in the 2D fluid

We have already noticed that the longitudinal phonon branches in the triangular Wigner lattice start at the zone centre with the dispersion form of the plasmon in $D = 2$. A full comparison of the excitations in the anharmonic solid near melting with the plasmon excitation in the fluid near freezing is given in figure 6. All the dispersion curves shown there are terminated at the upper edge of the single electron–hole pair continuum in the fluid.

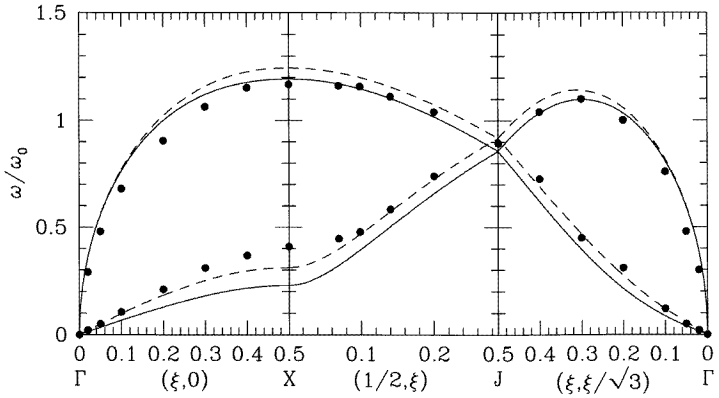

Figure 5. Phonon dispersion relations of the triangular electron lattice at $r_s = 40$ from $G_{pol}(k)$ (full curves) and from $G_{unpol}(k)$ (broken curves), compared with the results of harmonic calculations (dots). The direction of the wavevector $\boldsymbol{q}$, with components in units of $4\pi/(\sqrt{3}d)$, is shown below the graph. The frequencies are plotted as functions of ξ and are in units of $\omega_0 = [8e^2/(md^3)]^{1/2}$.

Table 3. Elastic constants c_{ij} (in units of $2e^2/(\pi d3)$) and the plasmon dispersion coefficient $A_{[10]}$ (in units of $2e^2/(\pi nmd^3)$) for the triangular Wigner electron lattice at $r_s = 40$.

		c_{11}	c_{33}	$A_{[10]}$
$G_{unpol}(k)$	LW		0.250	−1.56
	HD	0.749	0.444	
G_{pol}(k)	LW		0.123	−1.92
	HD	0.369	0.363	

To understand the information carried by figure 6 we first recall that, as discussed in detail elsewhere for the case of ^{4}He [25], the crystalline dispersion relations in equations (9) and (10) can be obtained by back-folding of the dispersion relation

$$\omega^2(k) = k^2F(k) = \frac{2\pi ne^2k}{m}f^2(k)[1 - G(k)] \tag{25}$$

into the first Brillouin zone. The mode frequency from equation (25) is shown in figure 6 together with the Feynman-like form of the dispersion relation for a fluid within a single-mode representation of the spectrum of density fluctuations

$$\omega^2(k) = -\frac{nk^2}{m\chi(k)}. \tag{26}$$

The main difference between these two expressions at the values of r_s of present interest arises from the Debye–Waller factor in equation (25), which depresses the collective mode frequency below the result in equation (26) at finite values of the wavenumber.

In a Bose system like ^{4}He this depression reflects multi-phonon modes overlying the single-mode dispersion curve and picking up oscillator strength as the wavenumber increases. However, in a Fermi system there is an opposite effect from the growth of oscillator strength in the single pair continuum underlying the collective mode. This is illustrated in figure 6 by reporting the dispersion relation calculated by Neilson *et al* [26]

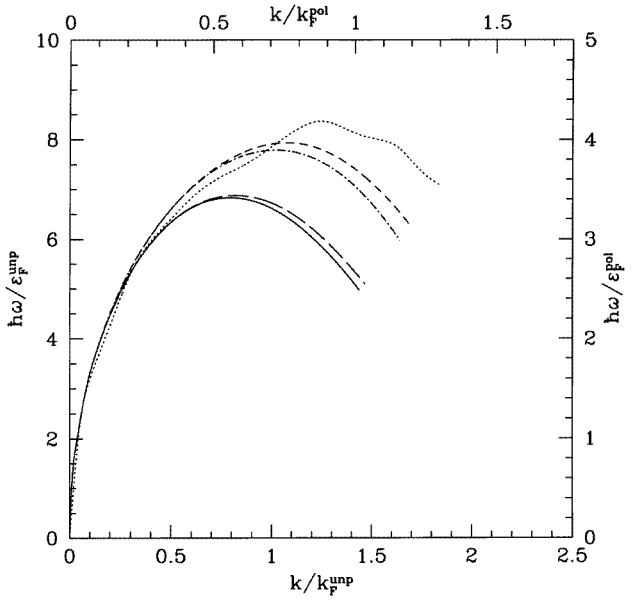

Figure 6. Dispersion relations for the collective mode in the 2D electron fluid near freezing. From bottom to top are shown the results of equation (25) using $G_{pol}(k)$ (full curve) and $G_{unpol}(k)$ (long-dashed curve), the results of equation (26) using $\chi_{pol}(k)$ (chain curve) and $\chi_{unpol}(k)$ (short-dashed curve) and the result of a direct calculation on the unpolarized fluid (dotted curve).

for the unpolarized electron fluid at $r_s = 35$ in $D = 2$. It is seen that, according to their result, the repulsion on the plasmon from the single pair continuum is dominant and leads to overshooting of the single-mode result in equation (26).

5. Concluding remarks

We have evaluated the phonon frequencies and the mechanical properties of ideal electron crystals near melting in the quantal regime using an approximate approach from density functional theory to account for exchange and correlation. For the BCC crystal we have been able to demonstrate convergence of a self-consistent phonon calculation and stability against elastic strains, under a rather wide range of choices for the inputs of the calculation. On the same grounds we can conclude that the FCC structure for the electron crystal, though energetically competitive with the b.c.c. structure at $r_s \approx 100$, is mechanically unstable under shear.

Our results allow less definite conclusions for the ideal 2D electron solid near melting. We found it to be mechanically stable at the expected value of the mean square particle displacement, though quantitatively the calculated values of the elastic constants are very sensitive to the details of the theory and to its inputs. Furthermore, a demonstration that a self-consistent phonon calculation beyond the simplest RHA can be brought to successful conclusion is still lacking. Anharmonicity in this system clearly deserves further and more refined theoretical study.

Acknowledgments

We are very grateful to Dr S Moroni for providing us with the results of his quantal Monte Carlo studies of the dielectric response function and the local field factor of strongly coupled electron fluids.

Appendix 1. The ideal contribution to the deformation work

An accurate treatment of the ideal kinetic energy functional is usually necessary in DFT calculations and is achieved by transforming the equilibrium condition given by equation (2) into a single-particle Schrödinger equation involving the Kohn–Sham effective potential defined there. However, in the very special case presented by a DFT calculation of phonon dispersion curves for a Wigner crystal at large values of r_s, the ideal contribution $\Delta\Omega_0$ to the deformation work can be shown to be essentially negligible.

We first estimate the consequences of the ideal term by treating the kinetic energy functional by the same type of truncated second-order expansion which has been used in treating the excess term in section 2 in the main text. It is easily seen that the effective force constants entering equation (9) are then shifted by an amount $\Delta F(k)$ given by

$$\Delta F(k) = -\frac{nf^2(k)}{m\chi_0(k)} \tag{A1.1}$$

where $\chi_0(k)$ is the Lindhard susceptibility for the ideal Fermi gas. Numerical evaluation shows that the vibrational frequencies are shifted by amounts of order 1–2% at values of r_s corresponding to melting both in $D = 3$ and in $D = 2$.

For a more transparent analytical estimate leading to essentially the same conclusion we resort next to a local density approximation for the kinetic energy functional:

$$T_0[n(\boldsymbol{r})] = \int \mathrm{d}\boldsymbol{r} n(\boldsymbol{r})\varepsilon_0(n(\boldsymbol{r})) \tag{A1.2}$$

with $\varepsilon_0(n)$ the kinetic energy per particle in an ideal Fermi gas at density n. By including a term from the third functional derivative of T_0 one easily finds

$$\Delta\Omega_0 = -\frac{1}{2}\alpha \int \mathrm{d}\boldsymbol{r}_1 \int \mathrm{d}\boldsymbol{r}_2 [n_d(\boldsymbol{r}_1)n_d(\boldsymbol{r}_2) - n_0(\boldsymbol{r}_1)n_0(\boldsymbol{r}_2)] \tag{A1.3}$$

where

$$\alpha = 2\frac{\mathrm{d}\varepsilon_0}{\mathrm{d}n} + 4n\frac{\mathrm{d}^2\varepsilon_0}{\mathrm{d}n^2} + n^2\frac{\mathrm{d}^3\varepsilon_0}{\mathrm{d}n^3} \tag{A1.4}$$

in $D = 3$ and

$$\alpha = 2\frac{\mathrm{d}\varepsilon_0}{\mathrm{d}n} \tag{A1.5}$$

in $D = 2$. These results correspond to shifts in $G(k)$ in equation (10) which are given by $-\beta(k/k_F)^2$ with $\beta = 2.53/r_s$ for a spin-polarized system in $D = 3$ and by $-\beta(k/k_F)$ with $\beta = 2/r_s$ for a spin-polarized system in $D = 2$. It is evident that at the critical value of r_s such shifts can only affect the calculated phonon frequencies at the level of a few per cent.

Appendix 2. Derivation of the RHA limit in $D = 3$

The dynamical matrix $D_{\alpha\beta}(\boldsymbol{q})$ corresponding to equations (9) and (10) in $D = 3$ is

$$D_{\alpha\beta}(\boldsymbol{q}) = \frac{1}{3}\omega_p^2\delta_{\alpha\beta} + \frac{1}{Nm}\sum_{\boldsymbol{R}\neq 0}[1 - \exp(\mathrm{i}\boldsymbol{q}\cdot\boldsymbol{R})]\frac{\partial^2\psi(\boldsymbol{R})}{\partial R_\alpha \partial R_\beta} \tag{A2.1}$$

where a Greek suffix denotes a Cartesian component, $\boldsymbol{R}$ are the lattice sites and $\psi(r)$ is the Fourier transform of the function $mF(k)$ defined in equation (10).

The expression (A2.1) has the same structure as the general result derived by Kugler [6] within the renormalized phonon theory. In his case the function $\psi(\boldsymbol{R})$ is given by

$$\psi_K(\boldsymbol{R}) = \exp\left(\sum_{\alpha\beta}\lambda_{\alpha\beta}(R)\nabla_\alpha\nabla_\beta\frac{e^2}{R}\right) \tag{A2.2}$$

where

$$\lambda_{\alpha\beta}(\boldsymbol{R}) = \langle u_\alpha(0)\mu_\beta(0)\rangle - \langle u_\alpha(0)u_\beta(\boldsymbol{R})\rangle \tag{A2.3}$$

$\boldsymbol{u}(\boldsymbol{R})$ being the fluctuation in the position of the particle associated with the lattice site $\boldsymbol{R}$.

In his RHA calculations to leading order Kugler neglected the inter-site term in equation (A2.3). Using $\langle u_\alpha(0)u_\beta(0)\rangle = \frac{1}{3}\langle u^2\rangle\delta_{\alpha\beta}$ for a cubic crystal, $\psi_K(\boldsymbol{R})$ reduces in this case to

$$\psi_K(\boldsymbol{R}) \to \exp\left[\frac{1}{3}\langle u^2\rangle\nabla^2\left(\frac{e^2}{R}\right)\right]. \tag{A2.4}$$

After Fourier transform equation (A2.4) yields a field of effective force constants given by

$$F_K(k) \to \frac{1}{m}f^2(k)\phi(k) \tag{A2.5}$$

which corresponds to equation (10) when the local field factor $G(k)$ is set equal to zero. Conversely, the above derivation shows that the local field factor in equation (10) effectively accounts in our DFT approach for inter-site correlations from data on the fluid phase near the freezing point.

Appendix 3. Asymptotic behaviours of the local field factor $G(k)$

The low-k behaviour of $G(k)$ is fixed by the compressibility sum rule [13], yielding

$$\lim_{k\to 0} G(k) = \gamma k^2 \tag{A3.1}$$

with

$$\gamma = (4\pi n^2 e^2)^{-1}\left(\frac{1}{K_0} - \frac{1}{K}\right) = -(4\pi e^2)^{-1}\left(n\frac{\mathrm{d}^2\varepsilon_{xc}}{\mathrm{d}n^2} + 2\frac{\mathrm{d}\varepsilon_{xc}}{\mathrm{d}n}\right) \tag{A3.2}$$

in $D = 3$ and

$$\lim_{k\to 0} G(k) = \gamma k \tag{A3.3}$$

with

$$\gamma = (2\pi n^2 e^2)^{-1}\left(\frac{1}{K_0} - \frac{1}{K}\right) = -(2\pi e^2)^{-1}\left(n\frac{\mathrm{d}^2\varepsilon_{xc}}{\mathrm{d}n^2} + 2\frac{\mathrm{d}\varepsilon_{xc}}{\mathrm{d}n}\right) \tag{A3.4}$$

in $D = 2$. In these equations K_0 is the compressibility of an ideal Fermi gas while K and ε_{xc} are the compressibility and the exchange and correlation energy per particle of

the interacting electron fluid. The exchange and correlation energy of the electron fluid is accurately known from QMC work [3–5].

The asymptotic behaviour of $G(k)$ in the limit of large k is instead fixed by the Kimball–Niklasson relation. In $D = 3$ one has [27]

$$\lim_{k\to\infty} G(k) = ak^2 + b \tag{A3.5}$$

with

$$a = \frac{\langle T - T_0\rangle}{6\pi ne^2} \tag{A3.6}$$

$$b = \frac{2}{3}[1 - g(0)] + \frac{4m}{\pi ne^2\hbar^2}\left(\frac{1}{5}\langle T^2 - T_0^2\rangle - \frac{1}{9}(\langle T\rangle^2 - \langle T_0\rangle^2)\right). \tag{A3.7}$$

Here, $\langle T^n\rangle$ are the moments of the kinetic energy of the interacting electron fluid and $\langle T_0^n\rangle$ are their counterparts in the ideal Fermi gas, while $g(0)$ is the contact value of the electron–electron pair distribution function. The corresponding relations in $D = 2$ are [28]

$$\lim_{k\to\infty} G(k) = ak + b \tag{A3.8}$$

with

$$a = \frac{\langle T - T_0\rangle}{3\pi ne^2} \tag{A3.9}$$

$$b = 1 - g(0). \tag{A3.10}$$

The first moment $\langle T\rangle$ is again known from the QMC data on the ground state energy [3–5], while the quantity $g(0)$ is zero in the spin-polarized fluid and is effectively zero in the unpolarized fluid near freezing. For the second moment $\langle T^2\rangle$ entering equation (A3.7) we have instead used a lower bound given by Holas [27] to estimate $b \approx 0.8$ in $D = 3$.

References

[1] Wigner E P 1934 *Phys. Rev.* **46** 1002
[2] Wigner E P 1938 *Trans. Faraday Soc.* **34** 678
[3] Ceperley D M and Alder B J 1980 *Phys. Rev. Lett.* **45** 567
[4] Tanatar B and Ceperley D M 1989 *Phys. Rev.* B **39** 5005
[5] Rapisarda F and Senatore G 1996 *Austr. J. Phys.* **49** 161
[6] Kugler A A 1969 *Ann. Phys., NY* **53** 133
[7] Platzman P M and Fukuyama H 1974 *Phys. Rev.* B **10** 3150
[8] Tosi M P and Tozzini V 1994 *Phil. Mag.* B **69** 833
[9] Tosi M P and Tozzini V 1993 *Europhys. Lett.* **23** 433
[10] Moroni S, Ceperley D M and Senatore G 1992 *Phys. Rev. Lett.* **69** 1837
[11] Moroni S, Ceperley D M and Senatore G 1995 *Phys. Rev. Lett.* **75** 689
[12] Ceperley D M 1978 *Phys. Rev.* B **18** 3126
[13] Singwi K S and Tosi M P 1981 *Solid State Phys.* **36** 177
[14] Born M and Huang K 1954 *Dynamical Theory of Crystal Lattices* (Oxford: Oxford University Press)
[15] Ferconi M and Tosi M P 1991 *J. Phys.: Condens. Matter* **3** 9943
[16] Ramakrishnan T V 1984 *Pramāna* **22** 365
[17] Senatore G and Pastore G 1990 *Phys. Rev. Lett.* **64** 303
[18] Clark C B 1958 *Phys. Rev.* **109** 1133
[19] Coldwell-Horsfall R A and Maradudin A A 1960 *J. Math. Phys.* **1** 395
[20] Carr W J Jr 1961 *Phys. Rev.* **122** 1437
[21] Houston W V 1948 *Rev. Mod. Phys.* **20** 161
[22] Betts D D, Bhatia A B and Wyman M 1956 *Phys. Rev.* **104** 37
[23] Bonsall L and Maradudin A A 1977 *Phys. Rev.* B **15** 1959
[24] Esfarjani K and Chui S T 1991 *J. Phys.: Condens. Matter* **3** 5825

[25] Tozzini V and Tosi M P 1995 *Europhys. Lett.* **32** 67
[26] Neilson D, Swierkowski L, Szimanski J and Liu L 1992 *J. Low Temp. Phys.* **89** 251
[27] Holas A 1986 *Strongly Coupled Plasma Physics* ed F J Rogers and H E DeWitt (New York: Plenum) p 463
[28] Yarlagadda S and Giuliani G F 1989 *Phys. Rev.* B **39** 3386